Microchimica Acta (2022) 189:395
https://doi.org/10.1007/s00604-022-05490-4

ORIGINAL PAPER

Electrochemical assay of acetamiprid in vegetables based on nitrogen-doped graphene/polypyrrole nanocomposites

Jiasheng Wang[1] · Decheng Zhang[1] · Keke Xu[1] · Ni Hui[1] · Dongwei Wang[1]

Received: 17 March 2022 / Accepted: 11 September 2022 / Published online: 28 September 2022

Abstract

Dual-mode electrochemical aptasensor based on nitrogen-doped graphene (NG) doped with the conducting polymer polypyrrole (PPy) nanocomposite is proposed for the determination of acetamiprid. NG/PPy was electrodeposited onto the glassy carbon electrode (GCE) using cyclic voltammetry technique. NG/PPy/GCE showed outstanding electrocatalytic activity for the oxidation of nitrite due to "active region" induced by the charge redistribution of carbon atoms. The ultrasensitive dual-mode biosensor for acetamiprid could be easily developed by coupling acetamiprid aptamers with the NG/PPy hybrid. The specific binding between acetamiprid and the aptamers resulted in the increase of differential pulse voltammetry (DPV) signal change and the decrease of chronoamperometry (CA) signal, and the concentration of acetamiprid could be measured. The working potentials of DPV and CA were − 0.2 ~ 0.4 V and − 0.4 ~ 0.4 V (vs. SCE), respectively. The dual-mode acetamiprid biosensor showed a wide linear range from 10^{-12} to 10^{-7} g mL^{-1}, with low detection limits of 1.15×10^{-13} g mL^{-1} and 7.32×10^{-13} g mL^{-1} through DPV and CA modes, respectively. Moreover, owing to high active area and superior conductivity, as well as good electrocatalytic ability, the dual-sensing platform based on NG/PPy nanocomposite supported the quantification of acetamiprid in complex samples.

Keywords Nitrogen-doped graphene · Polypyrrole · Electrochemical (bio-)sensor · Differential pulse voltammetry · Cyclic voltammetry · Acetamiprid · Dual mode

Introduction

Acetamiprid (ACE) is a widespread neonicotinoid insecticide with high efficiency [1]. Growing evidence shows acetamiprid not only has harmful effects on non-target organisms such as birds, fish, and bees, but also damages mammalian sperm function and embryonic growth [2–4]. Concerns about the potential health effects of the globalization of neonicotinoid insecticides are increasing.

To date, conventional instrumental approaches based on chromatographic technique, such as high-performance liquid chromatography and liquid/gas chromatographyemass spectrometry, were applied to detect acetamiprid residues in practical samples [5, 6]. However, these shortcomings, such as time-consuming, complex operation, and large-scale detection equipment, seriously limited the application of these methods in the field of on-site and real-time monitoring [7]. Electrochemical aptasensors for the assay of pesticide have attracted great attention because of their outstanding features such as high affinity, quick response, reproducible ability, and lower detection limit, as well as their mutual promotion with new micromachining technology [8–10].

Graphene-based functionalized nanomaterials have sparked much research interests in the field of electrochemical (bio-)sensors by virtues of flexibility, stability, stretchability, and high conductivity [11–13]. Especially, the nitrogen-doped graphene (NG) has higher electron activity, better stability, and greater reactivity than graphene itself, because nitrogen element supplies extra lone pair electrons for graphene and the wettability of graphene is improved [14–16]. Nitrogen doping could lead to a redistribution of the surface charge on the grapheme, increasing the free carrier density, and thus improving the catalytic activity of the graphene [17]. Moreover, NG could interact with biomaterials through stronger affinity,

✉ Ni Hui
huini1029@163.com

✉ Dongwei Wang
w88030661@163.com

[1] Qingdao Agricultural University, Qingdao 266109, China

leading to enhanced loading capacity of biomolecules [18]. Thus, NG can be used as an active electrode nanomaterial for the catalytic reaction or for the electrochemical assay of acetaminophen residues, dopamine, and DNA [19–21].

The conducting polymers have caught considerable attention in the field of the fabrication of electronic devices [22–25]. The combination of graphene and the conducting polymers can be a powerful means of preparing modified electrodes with high electrochemical performances. For instance, the conducting polymer polypyrrole (PPy), with environmental stability, high electrical conductivity, and flexibility, has been one of the most widely researched conducting polymers in designing bioanalytical sensors [26, 27]. However, the preparation of NG doped polypyrrole nanocomposites using simple electrochemical methods and their application for the detection of acetamiprid are quite rarely reported.

Since single-mode sensing methods are often limited by signal capacity and sole analytical information, dual-mode biosensors with high accuracy and reliability are increasingly favored [28]. Herein, we constructed a highly sensitive and reliable dual-mode biosensor based on NG/PPy for the assay of acetamiprid. NG not only provided more catalytic active sites, but also had a large number of functional groups (-COOH, -NH_2) for the immobilization of biomolecules. PPy can enhance the conductivity of hybrids and increase the specific surface area of nanomaterials by reducing the accumulation of NG [29]. NG/PPy with porous structure interconnected by the nanosheets showed enhanced electrocatalytic behavior for the oxidation of nitrite. The concentration of the acetamiprid could be monitored through both the changes of DPV peak current and the CA signal (Scheme 1). The CA method complemented the quantitative detection of acetamiprid by the DPV method, forming a dual-mode detection strategy. The dual-mode biosensors can supply more detection options and double checks, leading to more reliable and accurate analytical results, as well as high selectivity and stability.

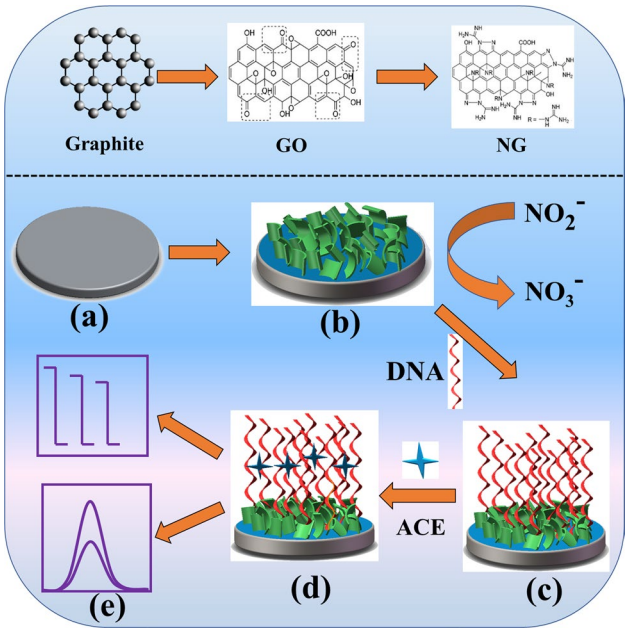

Scheme 1 The working principle of dual-mode biosensor based on NG/PPy nanocomposite. **a** Bare electrode; **b** NG/PPy/GCE; **c** DNA/NG/PPy/GCE; **d** ACE/DNA/NG/PPy/GCE; **e** the dual-mode output

Experimental section

Chemicals and apparatus

Flake graphite, $HONH_3Cl$, CH_7ClN_4, pyrrole, $CuSO_4$, citric acid, H_3PO_4(70%), KNO_3, and H_2SO_4 (98%) were obtained from Aladdin Regent (Shanghai, China).

For all electrochemical measurements, field emission scanning electron microscope (SEM), X-Ray photoelectron spectroscopy (XPS), Fourier transform infrared (FTIR), and X-ray diffraction (XRD), the required instruments and their models are listed in the supporting materials.

Preparation of NG/PPy nanocomposite

Graphene oxide (GO) and NG were synthesized using a modified Hummer's method according to previous reports [30, 31]. And the specific synthesis steps and details of GO and NG are shown in the Supplementary Materials. NG (10 mg) was dissolved in 5 mL ultrapure water. Then pyrrole (52.5 μL) was added to the NG solution and dissolved by ultrasound to obtain the deposition solution. NG/PPy nanocomposite was deposited onto the glassy carbon electrode (GCE) by cyclic voltammetry (CV, Fig. S1). CV parameters were set as follows: scanning range (− 0.2 ~ 1.2 V), scanning speed (0.1 V s^{-1}), and the number of cycles (15 cycles).

The electrochemical detection of nitrite

The catalytic ability of the NG/PPy nanocomposite for nitrite was investigated using the CV and I-T techniques. CVs were carried out in PBS (pH 7.4, 5 mL) before and after the addition of nitrite. The CV parameters were set in the scanning range from 0 to 1.2 V and the scanning speed of 0.1 V s^{-1}. The I-T was performed in PBS (pH 7.4, 5 mL) under the condition of continuous stirring at 0.8 V.

The dual-mode assay of acetamiprid

NG/PPy/GCE was immersed in PBS (pH 7.4, 0.2 M) containing 0.4 M EDC, 0.1 M NHS, and 10^{-6} M acetamiprid aptamers for 60 min, and then washed three times with water and PBS, respectively. The aptasensor (DNA/NG/PPy/GCE) was obtained. After DNA/NG/PPy/GCE was incubated in different concentration of acetamiprid for 30 min, DPVs were recorded in $[Fe(CN)_6]^{4-/3-}$ solution (5.0 mL, 5.0 mM) containing 0.1 M KCl. This was the first-mode of quantitative detection of acetamiprid. Meanwhile, after the capture of acetamiprid by the biosensor, the catalytic ability of the biosensor to nitrite was also weakened, and the catalytic current for the same amount of nitrite shown on the CA curves was also reduced, which was the second-mode of quantitative detection of acetamiprid (Scheme 1).

Details of the preparation and determination of vegetable samples are listed in the supporting materials.

Results and discussion

Characterization of NG/PPy nanocomposite

The surface morphology and microstructure of NG/PPy nanocomposite were characterized by SEM with an accelerating voltage of 5.0 kV. As shown in Fig. 1, obviously, the NG/PPy nanocomposite exhibited a nanosheet structure, and interlacing between the nanosheets created a three-dimensional porous structure. During the electrochemical polymerization of NG/PPy in a mixed solution containing pyrrole monomer and NG, the negatively charged NG with carboxyl groups could act not only as dopants to balance the positive charges in PPy chain, but also as "soft templates" to guide the growth of PPy. The NG dopant was the key factor to form the hierarchical porous morphology. Therefore, the interlaced-nanosheet structure of the NG/PPy nanocomposite provided a large surface area and more binding sites for the immobilization of biomolecules. The XRD patterns of NG and NG/PPy nanocomposites are shown in Fig. S2.

Characterization of the biosensor construction process

The formation of the NG/PPy nanocomposite and the successful immobilization of acetamiprid aptamers were confirmed by FTIR and XPS measurements. Figure 2A shows the FTIR spectra of the GO/PPy, NG/PPy, and DNA/NG/PPy. In the FTIR spectrum of GO/PPy, the peaks at 3446, 1364, and 1041 cm^{-1} were ascribed to O–H (stretching), C-O–H (bending vibrations), and C–O–C (stretching) groups, indicating that GO/PPy contained a large number of oxygen-containing functional groups [32, 33]. As the PPy skeleton contained the C-N bond and the N–H bond, the corresponding peaks appeared in 1111 and 1275 cm^{-1} of

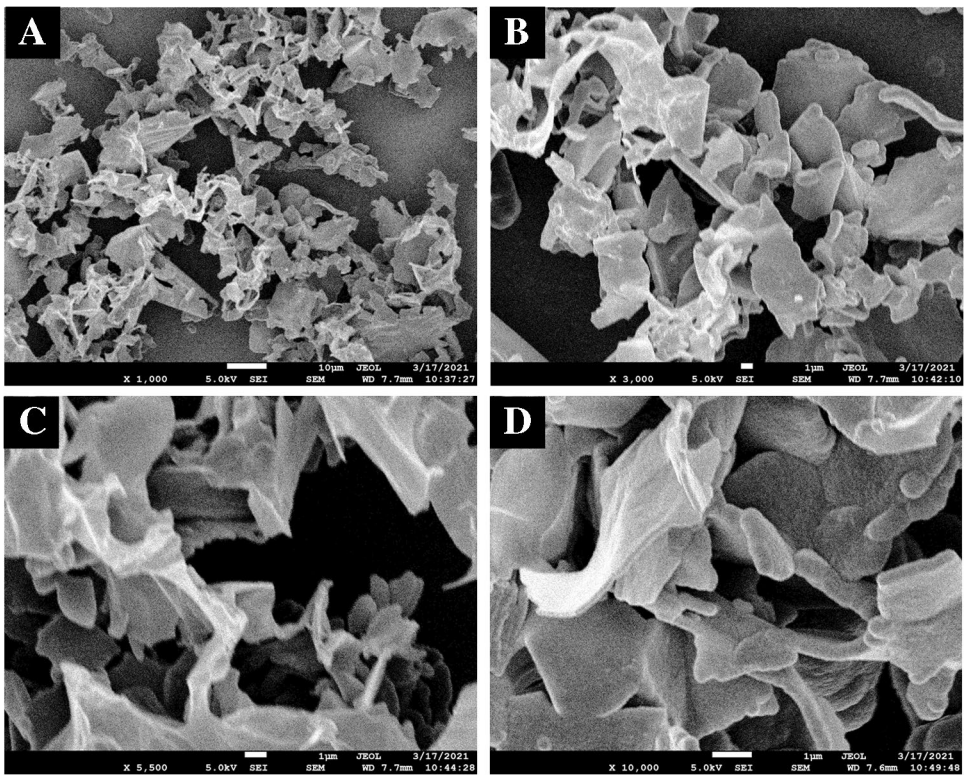

Fig. 1 The SEM images of NG/PPy nanocomposite at low and high magnification

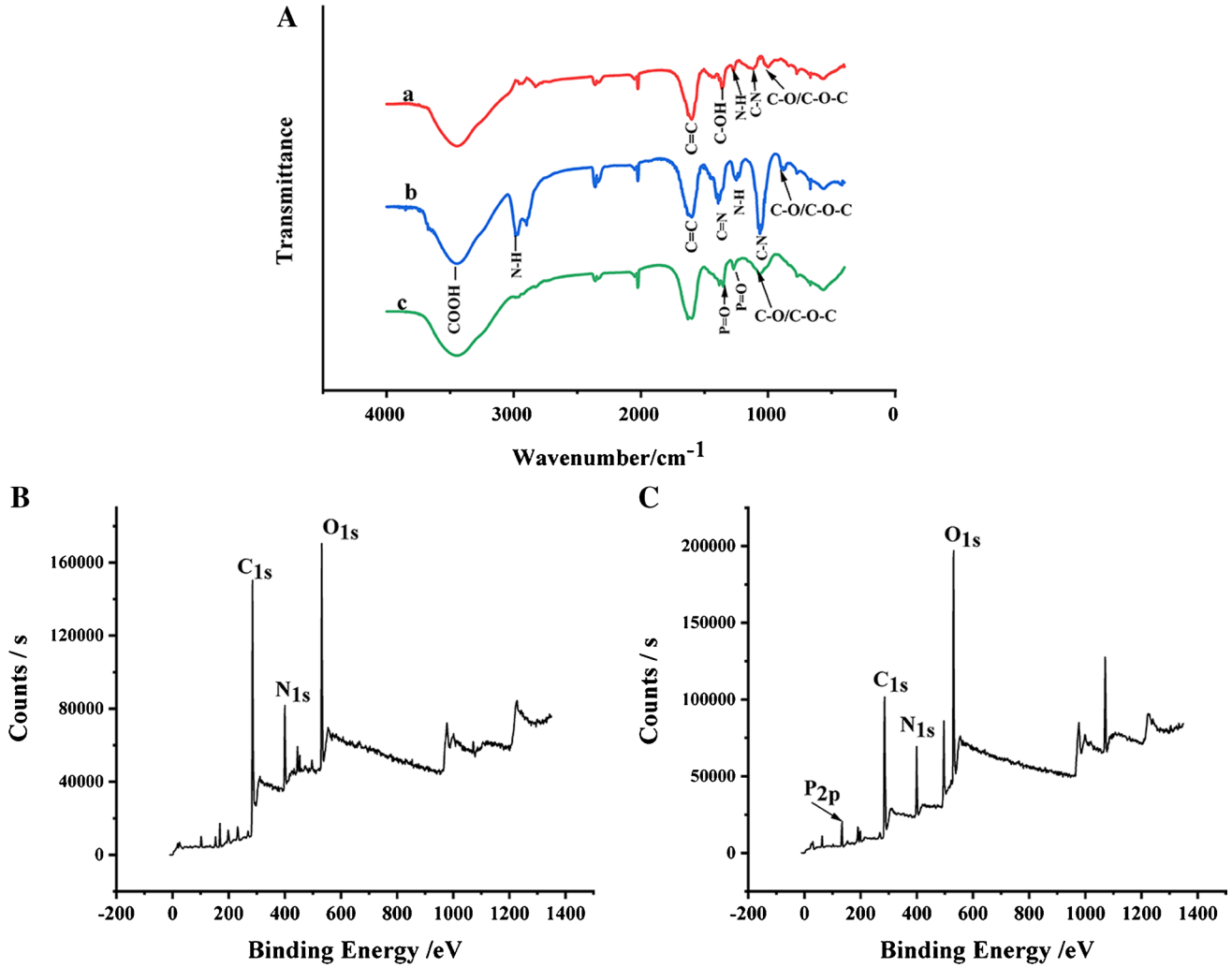

Fig. 2 (**A**) FTIR of GO/PPy (a), NG/PPy (b), and DNA/NG/PPy (c); XPS images of NG/PPy nanocomposite (**B**) and DNA/NG/PPy nanocomposite (**C**)

GO/PPy. In the FTIR spectrum of the NG/PPy nanocomposite (curve b), the new appearance of adsorption peaks at 1393 was due to the C = N bond. In addition, the peak values of the C-N bond and N–H bond increased significantly. The results strongly indicated the successful generation of N-doping structure of NG and the preparation of NG/PPy nanocomposite [34]. More interestingly, the new bands in the FTIR spectrum of DNA/NG/PPy appeared at 1273 and 1381 cm^{-1}, corresponding to the asymmetric stretching vibration and symmetric stretching vibration of the phosphate group. This indicated that DNA had been successfully attached to the modified electrode and the aptasensor has been successfully constructed.

The XPS measurements were also used to study the composition of the NG/PPy nanocomposite and the successful immobilization of acetamiprid aptamers. As shown in Fig. 2B, the fully scanned spectra of the NG/PPy nanocomposite contained C 1 s (284 eV), N 1 s (399.74 eV), and O 1 s (531.73 eV), which illustrated that the conducting polymer PPy (the source of C and N element) and NG (the only source of O element) were successfully synthesized into an integral composite. Comparing the XPS pattern of the NG/PPy nanocomposite (Fig. 2B) and the DNA/NG/PPy nanocomposite (Fig. 2C), it could be observed that after the immobilization of acetamiprid aptamers, the new peak (P 2p) appeared with the decrease of C 1 s peak and the increase of O 1 s, showing the successful attachment of acetamiprid aptamer. The quantitative analysis of the modified surfaces is shown in Table S1. The results showed that the nitrogen content of NG/PPY (13.48%) and DNA/NG/PPY (13.46%) was more than twice that of GO/PPY (6.36%), which fully proved the successful preparation of nitrogen doped graphene oxide.

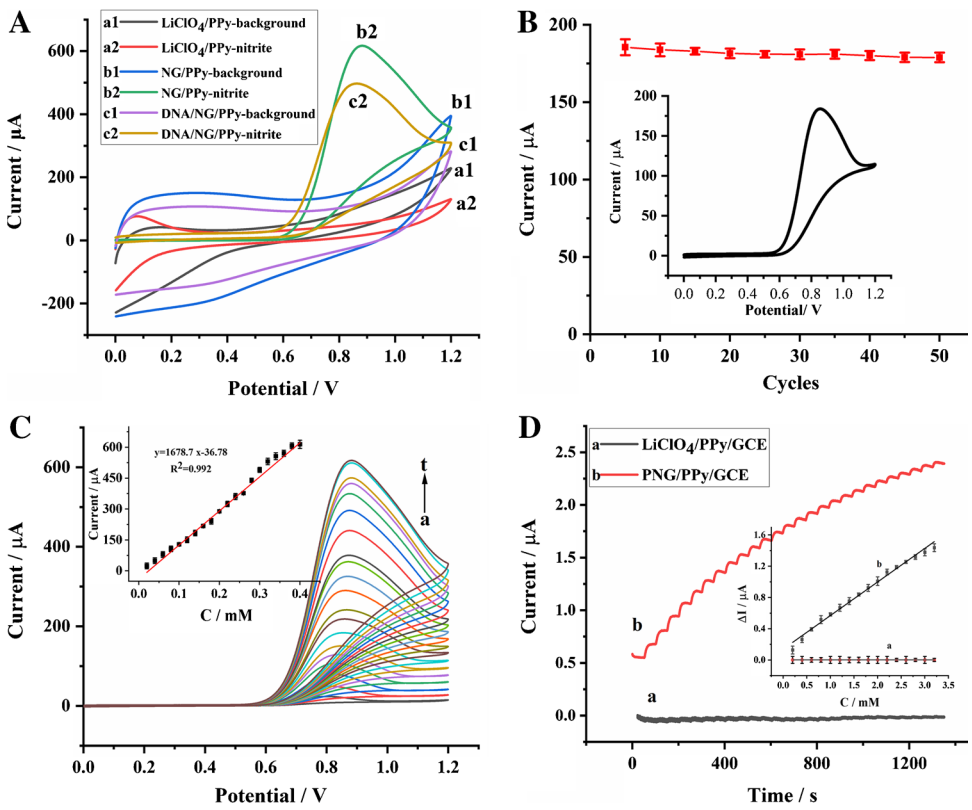

Fig. 3 (**A**) Cyclic voltammograms of $LiClO_4$/PPy/GCE (curve a1, a2), NG/PPy/GCE (curve b1, b2), and DNA/NG/PPy/GCE (curve c1, c2) in the absence (a1, b1, c1) and presence (a2, b2, c2) of 0.24 mM nitrite in PBS (pH 7.4) at scan rate of 0.1 V/s. (**B**) The stability experiment of NG/PPy/GCE for the oxidation of 0.12 mM nitrite (50 cycles of CVs) in PBS (pH 7.4) at scan rate of 0.1 V/s. (**C**) Cyclic voltammetry curve of nitrite (0.02–0.4 mM) catalyzed by NG/PPy/GCE (linear calibration curve in inset). (**D**) The I-T curves of $LiClO_4$/PPy/GCE (curve a) and NG/PPy/GCE (curve b) to successive addition of 0.2 mM nitrite into stirring PBS (5 mL, pH 7.4)

Catalytic property of NG/PPy/GCE for nitrite

The electrochemical oxidation of nitrite on $LiClO_4$/PPy/GCE, NG/PPy/GCE, and DNA/NG/PPy/GCE was investigated using CV and I-T techniques. Figure 3A shows that $LiClO_4$/PPy/GCE did not show any oxidation responses of nitrite, proving that nitrite could not undergo electrochemical oxidation on this surface (curve a1, a2). In contrast, an oxidation peak appeared on the NG/PPy/GCE and DNA/NG/PPy/GCE in the presence of nitrite, with the oxidation peak at about 0.85 V (curve b2, c2). Therefore, NG doped PPy could act as a catalyst for nitrite oxidation, in which NG played a key role. It could be observed from Fig. 3B that NG/PPy/GCE continuously oxidized nitrite for 50 cycles, and the well-defined and stable oxidation peak of nitrite remained unchanged, indicating that the NG/PPy/GCE had long-term stability for the oxidation capacity of nitrite.

Both CV and I-T techniques were performed to examine the sensitivity of NG/PPy/GCE toward the detection of nitrite under the optimum conditions. The CV response current increased with the nitrite concentration in the linear range of 0.02–0.40 mM with the linear equation ($i = 1678.73\ c - 36.78$, $R^2 = 0.991$), and NG/PPy/GCE displayed an excellent catalytic activity toward nitrite sensing with the detection limit of 0.017 mM (Fig. 3C). Amperometric I-T curves of $LiClO_4$/PPy/GCE and NG/PPy/GCE were obtained by injecting nitrite (0.2 mM) in magnetic stirring PBS (pH 7.4) at the constant potential of 0.8 V. As shown in Fig. 4D, $LiClO_4$/PPy/GCE showed almost no oxidation current towards the addition of nitrite while the NG/PPy/GCE displayed much larger response current towards nitrite, which was consistent with the results of CVs (Fig. 3A). The regression equation of $\Delta i = 0.409\ c + 0.176$ ($R^2 = 0.99$) was obtained with a linear range of 0.20–3.20 mM and the detection limit of 1.0 μM (S/N = 3). This superior sensing performance of NG/PPy/GCE for nitrite could be ascribed to the interlaced nanosheet microstructure, the excellent conductivity, and the large electroactive area.

Electrochemical construction process of the biosensor

Chronocoulometry (CC), CV, and EIS techniques were all used to characterize the nature of NG/PPy nanocomposite and the stepwise construction of the acetamiprid biosensor. CC is a convenient and valuable technique to estimate the electroactive area of the modified electrodes. According to the Cottrell equation $[Q(t) = (2nFAD^{1/2}\pi^{-1/2}C)\ t^{1/2} + Q_{dl} + Q_{ads}]$ [35], the electroactive area of the bare electrode, $LiClO_4$/PPy/GCE, NG/PPy/GCE, DNA/NG/PPy/GCE, and ACE/DNA/NG/PPy/GCE was calculated (refer to the supporting materials for the meaning of each parameter). Figure 4(A and B) shows that the slope of NG/PPy/GCE reached the maximum among the five electrodes, exhibiting

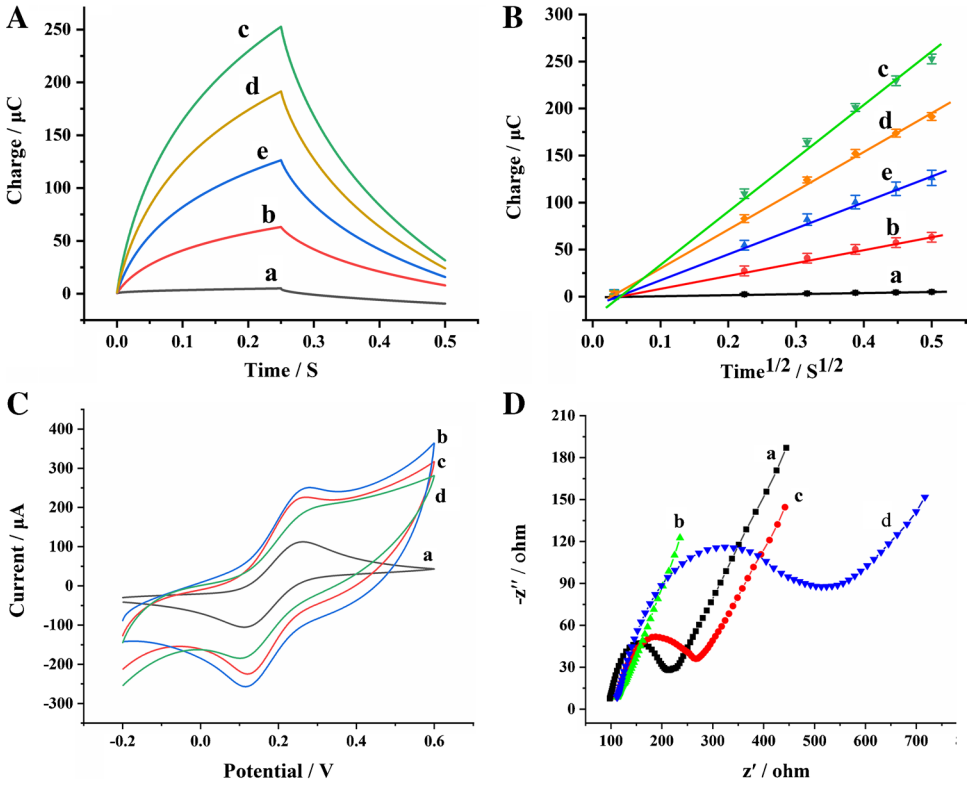

Fig. 4 CC (**A** and **B**) of the bare electrode (a), $LiClO_4$/PPy/GCE (b), NG/PPy/GCE (c), DNA/NG/PPy/GCE (d), and ACE/DNA/NG/PPy/GCE (e) recorded in 5 mM $[Fe(CN)_6]^{4-/3-}$; CV (**C**) and EIS (**D**) of the construction process of the biosensor in the solution containing 0.1 M KCl and equimolar 5 mM $[Fe(CN)_6]^{4-/3-}$ (a: the bare electrode; b: NG/PPy/GCE; c: DNA/NG/PPy/GCE; d: ACE/DNA/NG/PPy/GCE)

that the active area of NG/PPy/GCE (curve c) was the largest among them. The active surface area of the NG/PPy/GCE (curve c, 0.391 cm^2) was counted, which was 57 and 4 times larger than that of the bare GCE (curve a, 0.00684 cm^2) and the $LiClO_4$/PPy/GCE (curve b, 0.098 cm^2), respectively. More encouraging, with the immobilization of acetamiprid aptamer and the capture of acetamiprid molecules, the active areas of DNA/NG/PPy/GCE (curve d, 0.299 cm^2) and ACE/DNA/NG/PPy/GCE (curve e, 0.195 cm^2) decreased significantly, which was due to the non-conductivity of apatamer and acetamiprid. These results showed that NG/PPy nanocomposite could provide the large electroactive area for the immobilization of biomolecules, and the microstructure of NG/PPy nanocomposite revealed by SEM was further confirmed.

Figure 4C shows that NG/PPy/GCE (curve b) displayed much larger redox peak current than that of the bare electrode (curve a), indicating that the NG/PPy nanocomposite was excellently conductive. After the immobilization of acetamiprid aptamer on the surface of NG/PPy/GCE, the peak current of DNA/NG/PPy/GCE decreased (curve c), owing to the fact that large-sized and non-conductive DNA macromolecules greatly inhibited the electron transfer. As expected, a further decrease of the peak current was observed after the specific capture of acetamiprid with the biosensor (curve d).

The EIS plot included a semicircle whose chord length was equal to the resistance of electron transfer (Ret) [36]. Figure 4D illustrates that the NG/PPy/GCE was almost a straight line (curve b), indicating the excellent electron transfer ability of NG/PPy-modified electrode. The Ret values of DNA/NG/PPy/GCE and ACE/DNA/NG/PPy/GCE increased sharply in turn (159 and 417 Ω, curves c and d), which was ascribed to the electrostatic repulsion force between the negatively charged DNA and the negative $[Fe(CN)_6]^{3-/4-}$ probes and the successful formation of DNA-acetamiprid complexes.

Dual-mode detection of acetamiprid

The DPV technique was used under optimized conditions for quantitative measurement of acetamiprid. For a sufficiently specific binding between acetamiprid and the biosensor, the immobilization of the acetamiprid aptamer and the incubation time of acetamiprid were set to 60 min and 30 min, respectively (Fig. S5). Figure 5 shows the DPVs of different concentrations of acetamiprid on the biosensor, and the peak current decreased with the increase of acetamiprid concentration. A linear relationship between the signal inhibition rate ($\Delta I/I_0$) and acetamiprid concentration was obtained, with a wide linear range covering 6 orders of magnitude from 10^{-12} to10^{-7} g mL^{-1}. The linear fitting equation was $\Delta I/I_0 = 0.09645 \log c + 1.6292$ ($R^2 = 0.996$) (Fig. 5B), where I_0 represented the signal value without acetamiprid, and ΔI was the current change. The detection limit was calculated as 1.15×10^{-13} g mL^{-1} based on $3S_b/m$ (S_b and m were the

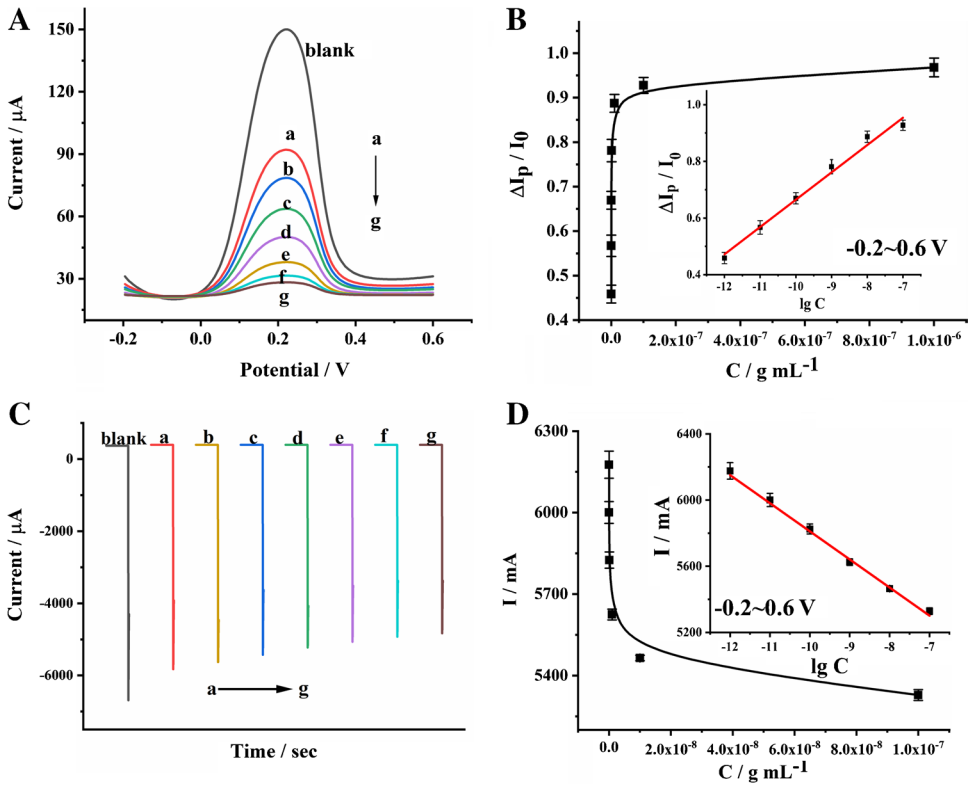

Fig. 5 **A** DPV curves of DNA/NG/PPy/GCE recorded in the solution containing 0.1 M KCl and equimolar 5 mM $[Fe(CN)_6]^{4-/3-}$ for detection of acetamiprid; **C** CA curves of DNA/NG/PPy/GCE recorded in the PBS (pH 7.4) containing 6 mM sodium nitrite (curves blank and a–g represented acetamiprid concentration of 0 and 10^{-12}–10^{-6} g mL^{-1}); **B**, **D** corresponding relationship between acetamiprid concentration and response signal (inset: the linear fitting equation). The working potentials of DPV and CA were − 0.2 ~ 0.4 V and − 0.4 ~ 0.4 V (vs. SCE), respectively

blank standard deviation of 10 repetitive blanks and the calibration curve slope, respectively).

The CA detection method of the biosensor was also investigated, while the response current of the biosensor to the same concentration of nitrite was recorded at different concentration of acetamiprid. In the CA detection mode, the response current produced by the nitrite decreased after the biosensor was incubated in acetamiprid (Fig. 5C), which was ascribed to the fact that the catalytic ability of the biosensor for nitrite was inhibited by acetamiprid. Figure 5D shows that the linear regression equation [$I = -169.94 \log c + 4111.6$, $R^2 = 0.994$] was obtained with the acetamiprid concentration within the range from 10^{-12} to 10^{-7} g mL^{-1}, and the LOD of the method is 7.32×10^{-13} g mL^{-1}. This dual-mode signal report could prove each other and enable more reliable detection. Compared with the other detection methods (Table S3), the dual-mode method showed a lower detection limit and a wider linear range. The excellent analytical performance of the biosensor may be attributed to its excellent conductivity, the high electroactive surface area, and the forceful combination between aptamer and acetamiprid.

Selectivity, stability, and reproducibility

If the biosensor could provide a platform with high selectivity for the target, the initial separation of samples could be avoided. To estimate the selectivity of the dual-mode biosensor, several kinds of interferents, such as maltose, ascorbic acid, saccharose, citric acid, NaCl, $CuSO_4$, chlorpyrifos, methyl parathion, fenitrothion, glyphosate, hydroquinone, catechol, rutin, urea, dopamine, and glucose, were investigated. At smaller concentration (10^{-9} g mL^{-1}) of acetamiprid, a larger $\Delta I_p/I_0$ was found for acetamiprid while much smaller changes were observed in 10^{-6} g mL^{-1} of the interferents (Fig. S6A). Figure S6B shows that the response current (I) to nitrite after incubation with acetamiprid changed greatly while that of the interferences remained basically unchanged. These results indicated that the dual-mode biosensor possessed excellent selectivity for acetamiprid.

The reproducibility of the constructed biosensor was tested through both intra- and inter-assays. The intra-assay was performed using the same batch of six biosensors for the detection of acetamiprid (10^{-9} g mL^{-1}), whereas the inter-assay was carried out in six different batches. For the DPV mode, 5.02% and 4.21% relative standard deviation (RSD) for intra-assay and inter-assay measurements were obtained, respectively. For the CA mode, 3.32% and 2.98% RSD of the intra-assays and the inter-assays were obtained. These results indicated high reproducibility of dual-mode biosensor. Moreover, after 10 days of continuous detection of acetamiprid (10^{-9} g mL^{-1}), the results of the DPV method and the CA method were 92% and 87% of the original value, respectively, hinting at a desirable level of stability.

Table 1 Determination of acetamiprid in vegetables ($n=3$)

Sample	HPCL method (μg/mL)		Sample	Biosensor method (ng/mL)				
	Detected	RSD (%)		Detected by DPV	RSD (%)	Detected by CA	RSD (%)	Coincidence rate (DPV/CA) %
1	0.012	4.5	1'	0.015	4.2	0.016	3.8	93.8
2	0.054	3.1	2'	0.058	5.1	0.056	4.7	103.6
3	0.57	2.7	3'	0.61	4.2	0.60	2.8	101.7
4	0.89	3.1	4'	0.93	4.1	0.94	3.9	98.9

RSD (%) ($n=3$), 1', 2', 3', and 4' samples were obtained by diluting 1, 2, 3, and 4 samples 1000 times

Real sample detection

To confirm the practical application of the dual-mode strategy in the assay of acetamiprid, the dual-mode detection results were compared with that of the typical high-performance liquid chromatography (HPLC) technique. HPLC technique was used to detect acetamiprid in vegetable extracts according to the previous reports [37, 38]. Acetamiprid in the same sample was detected by DPV and CA methods, respectively. The detection results of the two methods confirmed each other, and the coincidence rate (DPV/CA) between the detection results fell between 93.8 and 103.6% (Table 1). Furthermore, the dual-mode detection results were basically consistent with the detection results of HPLC, indicating that the application of the dual-mode biosensor for the detection of acetamiprid in real samples was practically achievable. According to the current GB 2763–2016 in China, the maximum residue limits of acetamiprid in vegetables are 1.0 mg L^{-1}. The detection limit of the dual-mode biosensor for vegetables was 1.15×10^{-7} mg L^{-1} and 7.32×10^{-7} mg L^{-1} (DPV and CA modes). The dual-mode biosensor could meet the requirement for the quantitative detection of residual acetamiprid in vegetables. It was pointed out that when this method was used to detect pesticide residues in actual samples, vegetable samples need to be processed cumbersome. This was far from the requirement of samples without pretreatment.

Conclusion

A dual-mode DPV and CA biosensor based on the NG/PPy nanocomposite has been constructed and exhibited high sensitivity and selectivity for the detection of acetamiprid. The NG/PPy nanocomposite was prepared by a one-step electrodeposition method, which combined with the advantages of NG (excellent catalytic ability) and PPy (good electrical conductivity). The dual-mode biosensor provided diversified analytical data for the detection of acetamiprid compared to single-mode method. It was expected that the dual-mode strategy using the NG/PPy platform could significantly improve the analysis efficiency and accuracy and pave a new way for the development of biosensors for pesticide residue analysis.

Supplementary Information The online version contains supplementary material available at https://doi.org/10.1007/s00604-022-05490-4.

Funding This work was funded by the National Natural Science Foundation of China (21705088), Shandong Provincial Key R & D Plan (Major Scientific and Technological Innovation Project) (2022CXGC010611, 2022CXGC010401, 2021CXGC010813), and Shandong Provincial Peanut Industry Technology System Project (SDAIT-04–09).

Declarations

Conflict of interest The authors declare no competing interests.

References

1. Qiao X, Xia F, Tian D, Chen P, Zhou C (2018) Ultrasensitive "signal-on" electrochemical aptasensor for assay of acetamiprid residues based on copper-centered metal-organic frameworks. Anal Chim Acta 1050:51–59
2. Shi X, Sun J, Yao Y, Liu H, Huang J, Guo Y, Sun X (2019) Novel electrochemical aptasensor with dual signal amplification strategy for detection of acetamiprid - ScienceDirect. Sci Total Environ 705:135905
3. Kong XP, Zhang BH, Wang J (2021) Multiple roles of mesoporous silica in safe pesticide application by nanotechnology: a review. J Agric Food Chem 69:6735–6754
4. Yan S, Meng Z, Tian S, Teng M, Yan J, Jia M, Li R, Zhou Z, Zhu W (2020) A neonicotinoid insecticides exposure cause amino acid metabolism disorders, lipid accumulation and oxidative stress in ICR mice. Chemosphere 246:125661
5. López-García M, Romero-González R, Lacasaña M, Frenich AG (2017) Semiautomated determination of neonicotinoids and characteristic metabolite in urine samples using TurboFlow coupled to ultra high performance liquid chromatography coupled to Orbitrap analyzer. J Pharm Biomed Anal 146:378
6. Zhang B, Pan X, Venne L, Dunnum S, Mcmurry ST, Cobb GP, Anderson TA (2008) Development of a method for the determination of 9 currently used cotton pesticides by gas chromatography with electron capture detection. Talanta 75(4):1055–1060
7. Chen H, Hu O, Fan Y, Xu L, Fu H (2020) Fluorescence paper-based sensor for visual detection of carbamate pesticides in food

based on CdTe quantum dot and nano ZnTPyP. Food Chem 327(4):127075
8. Madianos L, Tsekenis G, Skotadis E, Patsiouras L, Tsoukalas D (2017) A highly sensitive impedimetric aptasensor for the selective detection of acetamiprid and atrazine based on microwires formed by platinum nanoparticles. Biosens Bioelectron 101:268
9. Eissa S, Zourob M (2017) Selection and characterization of DNA aptamers for electrochemical biosensing of carbendazim. Anal Chem 89(5):3138
10. Kannan K, Radhika D, Nesaraj AS, Sadasivuni K, Reddy KR, Kasai D, Raghu AV (2020) Photocatalytic, antibacterial and electrochemical properties of novel rare earth metal oxides-based nanohybrids. Mater Sci Energy Technol 3:853–861
11. Xu T, Zhang Z, Qu L (2020) Graphene-based fibers: recent advances in preparation and application. Adv Mater 32(5):1901979
12. You R, Liu Y, Hao Y, Han D, You Z (2020) Laser fabrication of graphene-based flexible electronics. Adv Mater 32:2072112
13. Kim KT, Dao TD, Jeong HM, Anjanapura RV, Aminabhavi TM (2015) Graphene coated with alumina and its utilization as a thermal conductivity enhancer for alumina sphere/thermoplastic polyurethane composite. Mater Chem Phys 153:291–300
14. Shao YY, Sheng Z, Engelhard MH, Li GS, Lin YH (2010) Nitrogen-doped graphene and its electrochemical applications. J Mater Chem 20(35):7491–7496
15. Yang Z, Cao Y, Li J, Jian Z, Zhang Y, Hu X (2015) Platinum nanoparticles functionalized nitrogen doped graphene platform for sensitive electrochemical glucose biosensing. Anal Chim Acta 871:35–42
16. Jiang BB, Wei XW, Wu FH, Wu KL, Chen L, Yuan GZ, Dong C, Ye Y (2014) A non-enzymatic hydrogen peroxide sensor based on a glassy carbon electrode modified with cuprous oxide and nitrogen-doped graphene in a nafion matrix. Microchim Acta 181(11–12):1463–1470
17. Chen J, Han Y, Kong X, Deng X, Ji H (2016) The origin of improved electrical double-layer capacitance by inclusion of topological defects and dopants in graphene for supercapacitors. Angew Chem Int Ed 55(44):13822–13827
18. Oghli AH, Soleymanpour A (2021) Pencil graphite electrode modified with nitrogen-doped graphene and molecular imprinted polyacrylamide/sol-gel as an ultrasensitive electrochemical sensor for the determination of fexofenadine in biological media. Biochem Eng J 167:107920
19. Anuar NS, Basirun WJ, Ladan M, Shalauddin M, Mehmood MS (2018) Fabrication of platinum nitrogen-doped graphene nanocomposite modified electrode for the electrochemical detection of acetaminophen. Sens Actuators B 266:375–383
20. Chen M, Su H, Mao L, Guo MY, Tang J (2017) Highly sensitive electrochemical DNA sensor based on the use of three-dimensional nitrogen-doped graphene. Microchim Acta 185(1):51
21. Yu Y, Jiang C, Mo L, Tao L, Yan F (2016) Electrochemical determination of carbendazim in food samples using an electrochemically reduced nitrogen-doped graphene oxide-modified glassy carbon electrode. Food Anal Methods 10(5):1–9
22. Xu S, Shi XL, Dargusch M, Di C, Chen ZG (2021) Conducting polymer-based flexible thermoelectric materials and devices: from mechanisms to applications. Prog Mater Sci 121:100840
23. Lu H, Wang H, Yang L, Zhou Y, Xu L, Hui N, Wang D (2021) A sensitive electrochemical sensor based on metal cobalt wrapped conducting polymer polypyrrole nanocone arrays for the assay of nitrite. Microchim Acta 189(1):26
24. Hui N, Wang J, Wang D, Wang P, Luo X, Lv S (2022) An ultrasensitive biosensor for prostate specific antigen detection in complex serum based on functional signal amplifier and designed peptides with both antifouling and recognizing capabilities. Biosens Bioelectron 200:113921
25. Reddy KR, Hemavathi B, Balakrishna GR, Raghu AV, Naveen S, Shankar MV (2019) Organic conjugated polymer-based functional nanohybrids: synthesis methods, mechanisms and its applications in electrochemical energy storage supercapacitors and solar cells. Polym Compos Funct Nanopart 11:357–379
26. Jain R, Jadon N, Pawaiya A (2017) Polypyrrole based next generation electrochemical sensors and biosensors: a review. TrAC, Trends Anal Chem 97:363–373
27. Zhang D, Lang X, Hui N, Wang J (2022) Dual-mode electrochemical biosensors based on chondroitin sulfate functionalized polypyrrole nanowires for ultrafast and ultratrace detection of acetamiprid pesticide. Microchem J 179:107530
28. Ding C, Wang X, Luo X (2019) Dual-mode electrochemical assay of prostate-specific antigen based on antifouling peptides functionalized with electrochemical probes and internal references. Anal Chem 91(24):15846–15852
29. Teng H, Song J, Xu G, Gao F, Luo X (2020) Nitrogen-doped graphene and conducting polymer PEDOT hybrids for flexible supercapacitor and electrochemical sensor. Electrochim Acta 355:136772
30. Wang X, Ding Y, Lu H, Chen F, Zhang N, Ma M (2018) Chemoselective solution synthesis of pyrazolic-structure-rich nitrogen-doped graphene for supercapacitors and electrocatalysis. Chem Eng J 347:754–762
31. Marcano DC, Kosynkin DV, Berlin JM, Sinitskii A, Sun Z, Slesarev A, Alemany LB, Lu W, Tour JM (2010) Improved synthesis of graphene oxide. ACS Nano 4(8):4806–4814
32. Raghu AV, Gadaginamath GS, Aminabhavi TM (2005) Synthesis and characterization of novel polyurethanes based on 1,3-bis(hydroxymethyl) benzimidazolin-2-one and 1,3-bis(hydroxymethyl) benzimidazolin-2-thione hard segments. J Appl Polym Sci 98(5):2236–2244
33. Raghu AV, Gadaginamath GS, Mathew NT, Halligudi SB, Aminabhavi TM (2007) Synthesis and characterization of novel polyurethanes based on 4,4′-[1,4-phenylenedi-diazene-2,1-diyl] bis(2-carboxyphenol) and 4,4′-[1,4-phenylenedi-diazene-2,1-diyl]bis(2-chlorophenol) hard segments. React Funct Polym 67(6):503–514
34. Zhang C, Rui H, Liao H, Hou Y (2013) Synthesis of amino-functionalized graphene as metal-free catalyst and exploration of the roles of various nitrogen states in oxygen reduction reaction. Nano Energy 2(1):88–97
35. Liu S, Ma Y, Cui M, Luo X (2018) Enhanced electrochemical biosensing of alpha-fetoprotein based on three-dimensional macroporous conducting polymer polyaniline. Sens Actuators B 255:2568–2574
36. Hui N, Sun X, Niu S, Luo X (2017) PEGylated polyaniline nanofibers: antifouling and conducting biomaterial for electrochemical DNA sensing. ACS Appl Mater Interfaces 9(3):2914–2923
37. Jin D, Xu Q, Yu L, Mao A, Hu X (2016) A novel sensor for the detection of acetamiprid in vegetables based on its photocatalytic degradation compound. Food Chem 194:959–965
38. Tang X, Li X, Ma D, Lu L, Qu B (2018) A label-free triplex-to-G-qadruplex molecular switch for sensitive fluorescent detection of acetamiprid. Talanta 189:599–605